A Hybrid Parting Method Based on Iterative Surface Growth Algorithm and Geometric Mouldability

Zhiqiang Zhao[1], Jerry Y. H. Fuh[2] and Andrew Y. C. Nee[3]

[1]National University of Singapore, q0306311@nus.edu.sg
[2]National University of Singapore, mpefuhyh@nus.edu.sg
[3]National University of Singapore, mpeneeyc@nus.edu.sg

ABSTRACT

A parting methodology to identify cavity and core surfaces, outer and inner parting lines, and undercut features based on surface topology and mouldability reasoning is presented in this paper. The approach first determines a cavity seed surface and a core seed surface. Then, the cavity and core surface groups are searched using the proposed iterative surface growth algorithm. Meanwhile, a concept of pseudo-straddle surface is introduced to deal with model geometry imperfection and free-form surfaces with imperfect draft angles. Subsequently, the outer and inner parting lines are identified using the proposed algorithms and criteria. The undercut features are finally identified based on the results of parting lines and associated surfaces. Since the approach is fully independent of the complexity of the geometry structure, it thus gives satisfactory results for models with complex geometry features.

Keywords: Injection mould, parting methodology, mouldability, geometry and topology.

1. INTRODUCTION

For a given moulding, the moulded part is formed between the core and cavity inserts. The pull direction along which the core and cavity inserts are opened is called the parting direction (P_D). P_{D+} is the moving direction of cavity insert, while P_{D-} represents the open direction of core insert. All surfaces moulded by the cavity are designated as cavity surfaces, and those surfaces moulded by the core, as core surfaces. The convex and concave portions of the moulding are considered as undercut features composed of undercut surfaces. Parting lines are defined as the intersection boundaries between the core, cavity and undercut surfaces. In principle, there are two types of parting lines, i.e. inner parting lines (**IPL**) and outer parting lines (**OPL**). **OPL** is the largest parting line loop, while **IPL** are other parting line loops located inside the body of the model. The cavity and core surfaces, **OPL** and **IPL**, and undercut features are key inputs for generation of parting surfaces, shut-off surfaces, the cavity and core inserts, and their side-cores and side-cavities in an intelligent mould design system.

The vast amount of literatures on automatic determination of parting lines, recognition of undercut features for injection moulded parts have been reported in the recent years. As the elemental geometry approach, V-Map and G-Map [4] concepts have been widely applied in determining parting lines, undercut features and have provided the fundamental criteria of mouldability of surfaces in an injection mould. Tan et al. [9] classified all the part surfaces into visible and invisible surfaces for a given parting direction based on the surface normal and the parting direction. If the surface normal contains positive vector components in the parting direction, the surface is visible. If the surface normal contains negative vector components, the surface is then invisible. When an edge is shared by a visible surface and an invisible surface, it is considered as a tentative parting edge. A series of these tentative parting edges, when properly connected, may form the required parting. Several similar approaches have been developed by [2], [6] and [10]. More recently, M.A. Rubio Paramio et al. [5] proposed a systematic approach for the automatic analysis of the mouldability of a paer based on visualization techniques, including slicing by parallel planes, scan line segment and Z-buffer methods. It was able to determine undercut features and the parting lines geometrically for a moulded part.

Graph-based feature recognition approaches have been successfully applied in identifying undercut features and parting lines for injection moulds. Contributions have been made by many researchers, e.g. [1], [7], [11] etc. In these approaches, a model is organized into a graph structure using B-Rep entities (surfaces, edges and vertices). The

geometric entities are expressed as nodes and the connectivity between any of the two entities as arcs in the graph. The graph is then split into sub-graphs using graph manipulation algorithms and mapped with those pre-defined graph patterns of known machine features. Fu et al. [3] developed a graph-based feature recognition methodology to detect possible undercuts using the rule-based approach based on the definitions, classification and criteria of the common types of undercut features of moulded products. More recently, Pralay Pal et al. [8] introduced a genetic algorithm to recognize undercut features. The algorithm extends the capability of rule-based feature recognition by allowing natural rule selection and adopting parallel searching for the emergence of better matching results during the parting process.

The survey of the previous work shows that the problems arising from CAD of injection moulds have generated a great deal of interest and some pioneering works in solving these problems have been done. They have provided good references for this paper although there are some limitations from the practical industrial application viewpoint. Firstly, few studies have considered model geometry and draft angle imperfections. Therefore, the methodologies are not robust for those products with geometry imperfections commonly appear in industrial products. Secondly, graph-based methodology could also fail in case of geometry imperfections and complex geometry composed of free-form surfaces since the sub-graphs derived from these models are not perfect so that the graph of undercut features cannot match with predefined sub-graphs. Thirdly, better results of the visibility and mouldability could be drawn if a moulding surface is analyzed globally from the view of the entire model rather than only among its adjacent surfaces locally for a given parting direction. Moreover, effective algorithms should be developed to implement the processes as well.

2. SURFACE CLASSIFICATION BASED ON GEOMETRY VISIBILITY AND MOULDABILITY

Essentially, the parting analysis is related to the surface visibility and mouldability information along the given parting direction. In this paper, a surface of a body is classified into one of the four categories (G_+, G_-, G_0, and G_s) according to its geometry characteristics and mouldability. Tab. 1 describes the definition of each group and the relevant algorithms to determine which group a surface should be classified into.

Surface categories	Description of algorithms
G_+	$N_i \bullet P_{D+} \geq 0$ for $i=1, 2, 3, \ldots n$
	$F_{intersect}(S, R_j, P_{D+}) \equiv NULL$ for $j=1, 2, 3, \ldots m$
G_-	$N_i \bullet P_{D-} \geq 0$ for $i=1, 2, 3, \ldots n$
	$F_{intersect}(S, R_j, P_{D-}) \equiv NULL$ for $j=1, 2, 3, \ldots m$
G_0	$N_i \bullet P_D \equiv 0$ for $i=1, 2, 3, \ldots n$
G_s	$N_i \bullet P_{D+} > 0$ for $i=1,2,3,\ldots k$ (for some normal vectors of triangulation pieces of surface **F**)
	$N_i \bullet P_{D-} > 0$ for $i=1,2,3,\ldots l$ (for other normal vectors of triangulation pieces of surface **F**)

Tab. 1: Surface classification based on geometry visibility and mouldability (modified from [2]).

In the above table, N_i represents the normal vector of ith planar triangular piece of a surface. n is the total number of triangular pieces after the triangulation process. $F_{intersect}$ is the intersected surfaces among an array of rays R and the part body towards either P_{D+} or P_{D-}. R_j represents the jth ray at the jth position of the 2D projection region of a surface at P_D. m is the total number of locations of the projected region of a surface to define the array of rays R.

Based on the definitions of different categories in Tab. 1, a surface in the group of G_+ satisfies two conditions, i.e. (i) all the normal vectors of planar triangular pieces contained by the surface have positive vector products towards P_{D+}, and (ii) no other surfaces exist inside the 2D projected region of the surface towards P_{D+}. It implies that this surface is not only geometrically visible but also not blocked by any other surfaces moving away towards P_{D+}; therefore, it is a potential cavity surface. Similarly, a surface in the group of G_- is geometrically visible and will not be blocked by any other surfaces towards P_{D-}; it is, therefore, a potential core surface. A surface in the group of G_0 is a zero draft surface. All the normal vectors of planar triangular pieces contained by this surface have a zero vector product with P_D. It could be further identified as a cavity surface, a core surface or an undercut surface based on the proposed searching approach and criteria. Lastly, a surface in the group of G_s is invisible along both P_{D+} and P_{D-} geometrically because the normal vectors of planar triangular pieces contained by this surface give positive vector products for both P_{D+} and

P_D directions. It is obviously a potential undercut surface. However, it could still be identified as a cavity surface or a core surface as long as it satisfies the definition of a pseudo-straddle surface and relative conditions to be discussed later.

2.1 Determination of the Parameter *'n'* and Normal Vector *'N'*

In Tab. 1, the parameter *'n'* is the total number of normal vectors which are used to determine the geometrical visibility of a targeted surface along the parting direction. *N* represents a normal vector of planar triangular pieces contained by the surface. There exist two cases as belows:

- For a planar surface, *n* equals to 1 and *N* is the normal direction of the plane as shown in Tab. 2. Here, the triangulation process is not necessary.
- All other surfaces are then considered as free-form surfaces in this paper. In these cases, *n* is the number of planar triangular pieces after the triangulation process of a surface in B-Rep. N_i represents the normal vector of *ith* triangular piece. Tab. 2 also illustrates the triangulation results of typical geometric surfaces, including cylindrical, conic, free-form and straddle surfaces.

Surface types	Planar surface	Cylindrical surface	Conic surface	Free-form surface	Straddle surface
Surface geometry					
Triangulation process	Not applied				
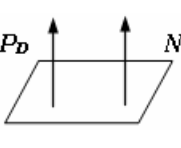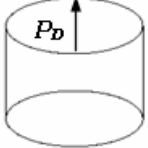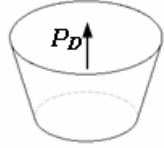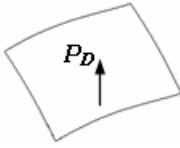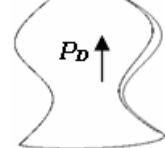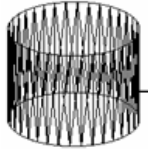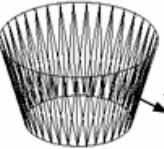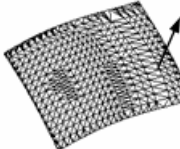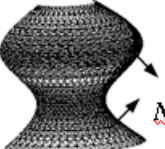
Tab. 2: Determination of the normal vectors by triangulation process for different kinds of surfaces.

2.2 Determination of Parameter *'m'* and the Array of Rays *'R'*

Different from *'n'*, the parameter *'m'* is the total number of locations where the array of rays *R* are generated in order to find the intersected surfaces with the targeted surface towards the given parting direction. It determines whether there exist other surfaces inside the 2D projected region of the targeted surface blocking its movement towards the given parting direction. Fig. 1 illustrates the three steps of the algorithm to determine *'m'* and *'R'*.

<u>Step 1</u>: The surface **F** is first projected onto a plane perpendicular to P_D. As a result, a 2D projected region R_P of **F** is drawn as shown in Fig. 1(a). It is expressed as

$$R_P = \{B_i\} \qquad \text{for } i=1,2,\ldots\text{numBoundry} \qquad (2.1)$$

Where, B_i is the *i*th closed boundary of the 2D region and numBoundry the total number of boundaries.

<u>Step 2</u>: A regular triangle net N_r is then created according to the boundary of the 2D region from step 1 in terms of the given accuracy as shown in Fig. 1(b).

$$N_r = \{M[i][j]\} \qquad \text{for } i=0,1,2,\ldots m\text{-}1; \ j=0, 1,2,\ldots n\text{-}1 \qquad (2.2)$$

Where *M* represents the position of the triangle net. $M[0][0] = \{X_{\min}, Y_{\min}\}$ and $M[m-1][n-1] = \{X_{\max}, Y_{\max}\}$. X_{min}, Y_{min} X_{max} and Y_{max} represent the containing boundary of the 2D region R_P.

<u>Step 3</u>: The array of rays *R* are constructed by mapping region R_P with N_r shown in Fig. 1(c).

$$R = \{M \mid M[k] \in R_P, P_{D+} \mid P_{D-}\} \qquad \text{for } k=1,2,\ldots m \qquad (2.3)$$

Where, m is the total number of the mapping points located inside the 2D region and the array of rays R is constructed by the position of $M[k]$ and the given parting direction.
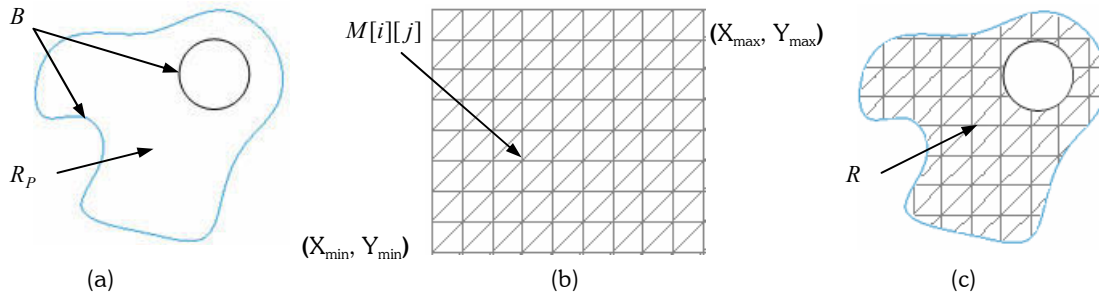
Fig. 1: Determination of the parameter 'm' and the array of rays 'R'' – (a) 2D projected region R_P , (b) regular triangle net N_r , (c) mapping points of R .

3. THE PROPOSED PARTING METHOD

3.1 Findings and Criteria of Parting in a Moulded Part

After studying industrial products and practices carefully, the parting of an injection moulded part should satisfy a few criteria and shows some characteristics based on their mouldability, graphic visibility and surface geometry topology for a given parting directions $\boldsymbol{P_{D+}}$ and $\boldsymbol{P_{D-}}$ respectively as follows:

- A cavity surface can be drawn away along $\boldsymbol{P_{D+}}$. Therefore, it is visible and not blocked by obstacle surfaces towards $\boldsymbol{P_{D+}}$. Similarly, a core surface should be visible and no obstacle surfaces towards $\boldsymbol{P_{D-}}$.
- All the cavity surfaces should connect each other and form a single group named the cavity surface group, while all core surfaces form a connective group named as the core surface group. This is restricted by the structure of a single injection mould, or lese the profiles of cavity and core cannot be sewn together nicely.
- A potential undercut surface is the one which fails to be identified as either a cavity or a core surface. It could be either a straddle surface or a surface which id not able to be drawn along either $\boldsymbol{P_{D+}}$ or $\boldsymbol{P_{D-}}$.
- Parting lines are the intersection among core, cavity and undercut surfaces. **OPL** loop has the maximal projected area at the plane perpendicular to $\boldsymbol{P_D}$, while **IPL** loops are those whose projection areas are smaller. There is only one **OPL** loop and maybe a few **IPL** loops in a molding [7].
- An undercut feature is always isolated by one or more **IPL** loops and **OPL** loop and can subsequently be identified according to the results of parting lines and the mouldability of associated surfaces.

3.2 Flow Chart of the Parting Methodology

The proposed parting methodology can be divided into three major processes as illustrated in Fig. 2, i.e. (1) identification of cavity and core surface groups, (2) identification of parting lines and (3) extraction of undercut features and revision of cavity and core surfaces.

There are two steps in the process of surface group identification. A cavity seed surface and a core seed surface are first pre-determined. In the second step, starting from the cavity and core seed surfaces respectively, a cavity surface group and a core surface group are searched using the proposed iterative surface growth algorithms. During the process, zero draft surfaces and pseudo-straddle surfaces are also manipulated using the proposed algorithms in order to enhance the results and deal with geometry imperfections. A zero draft surface could be identified as either a cavity surface or a core surface according to its topological relationship and mouldability properties. Pseudo-straddle surfaces are analyzed according to their geometry topology information and the given accuracy. After that, a nominated cavity surface group and a core surface group are defined as well as those remaining undefined surfaces in a model body.

Fig. 2 describes the four steps of parting lines identification. First, all the potential parting lines loops from the cavity surface group and the core surface group are extracted and further classified as tentative cavity parting line loops and core parting line loops. In step 2, two tentative **OPL** loops from the cavity side and the core side are found based on the largest projection area criterion. The other parting line loops are all set as **IPL** loops. Subsequently, the two **OPL**

loops are optimized based on the proposed criteria and algorithms presented later. Finally, all **IPL** are optimized and refined using the proposed methods. The final outputs are one **OPL** loop and a few **IPL** loops.

In the last process, the cavity surface group and the core surface group are revised according to the identified parting line loops. All undefined surfaces are assigned as undercut surfaces, and then regrouped into different sub-groups according to their connectivity. Each isolated undercut surface group therefore forms an undercut feature. As a result, all the surfaces of the model are fully defined using a cavity surface group, a core surface group, several undercut features. There are also a unique **OPL** loop and a few **IPL** loops.

Process 1: Identification of cavity and core surface groups

1: Determine cavity seed surface and core seed surface
2: Search cavity surface group and core surface group using iterative surface growth algorithm

Output: A cavity surface group + a core surface group

Process 2: Identification of parting lines

1: Get all boundary loops from cavity surface group and core surface group
2: Get two nominated **OPL** loops and other **IPL** loops
3: Optimize and get unique **OPL** loop
4: Optimization of **IPL** loops

Output: One *OPL* loop + a few *IPL* loops

Process 3: Extraction of undercut features and revision of cavity and core surfaces

1: Revise cavity surfaces and core surfaces
2: Identification of undercut features

Output: cavity surfaces + core surfaces + undercut features

Fig. 2: Flow chart of the proposed parting methodology.

3.3 Determination of Cavity Seed Surface and Core Seed Surface

A pre-defined cavity seed surface or a core seed surface will be used as a seed surface searching for all other cavity surfaces or core surfaces respectively. Therefore, it must be a confirmed cavity or core surface. The cavity seed surface $F_{CavitySeed}$ and the core seed surface $F_{CoreSeed}$ are determined in terms of the below conditions:

$$F_{CavitySeed} = \{F \mid F \in G_+ \cap F_{Adjancent} \in (G_+ \| G_0)\} \tag{3.1}$$

$$F_{CoreSeed} = \{F \mid F \in G_- \cap F_{Adjancent} \in (G_- \| G_0)\} \tag{3.2}$$

Where, $F_{Adjancent}$ represents all adjacent surfaces of a nominated surface.

If the cavity seed surface or the core seed surface cannot be obtained automatically, an interactive operation is needed to prompt the user choosing either a cavity seed surface or a core seed surface.

3.4 Search Cavity and Core Surface Groups Using Iterative Surface Growth Algorithm

Fig. 3 introduces the iterative surface growth algorithm used to search for the cavity surface group. It starts from the cavity seed surface. All adjacent surfaces $\mathbf{F_a}$ of the surface $\mathbf{F}$ are then passed through by cycling its boundary loops $\mathbf{L}$[iLoop] and associated edges $\mathbf{E}$[iEdge] in each loop. If an adjacent surface $\mathbf{F_a}$ is verified as a new cavity surface using the algorithm in Fig. 4, it will be added to the cavity surface list *pCavitySurface* and assigned as a new seed surface $\mathbf{F}$ for another around of searching iteratively. Subsequently, the cavity surface group will grow gradually from the cavity seed surface till the searching is complete. It is noted that all cavity surfaces are connected with each other.

The algorithm to verify whether an adjacent surfaces F_a is a valid new cavity surface is described in Fig. 4. Obviously, the surface cannot be a new cavity surface if it has been already an existing cavity surface. Or else, F_a can be classified into four cases based on its surface categories described in Tab. 1, i.e. G_+, G_-, G_0, and G_s respectively. If it is a G_+ surface, then F_a will be identified as a new cavity surface. While if it is a G_- surface, it is definitely not a new cavity surface. If this is G_0 surface, an algorithm introduced in 3.4.2 is used to determine whether it can be identified as a new cavity surface. If this is a G_s surface, another algorithm described in 3.4.1 is used to determine whether it can be identified as a new cavity surface.
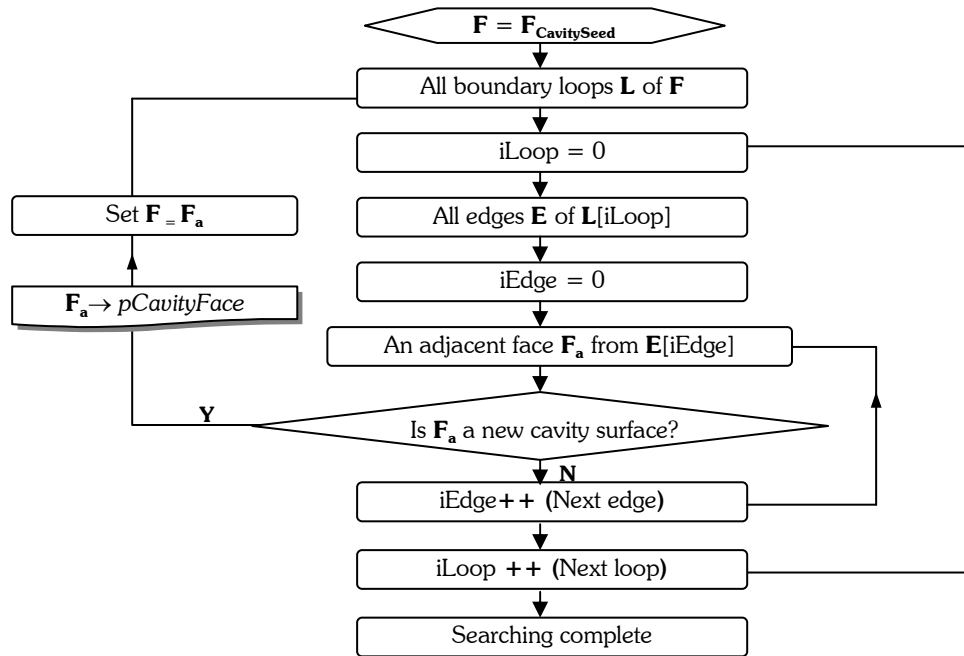
Fig. 3: Iterative surface growth algorithm for searching cavity surface group.
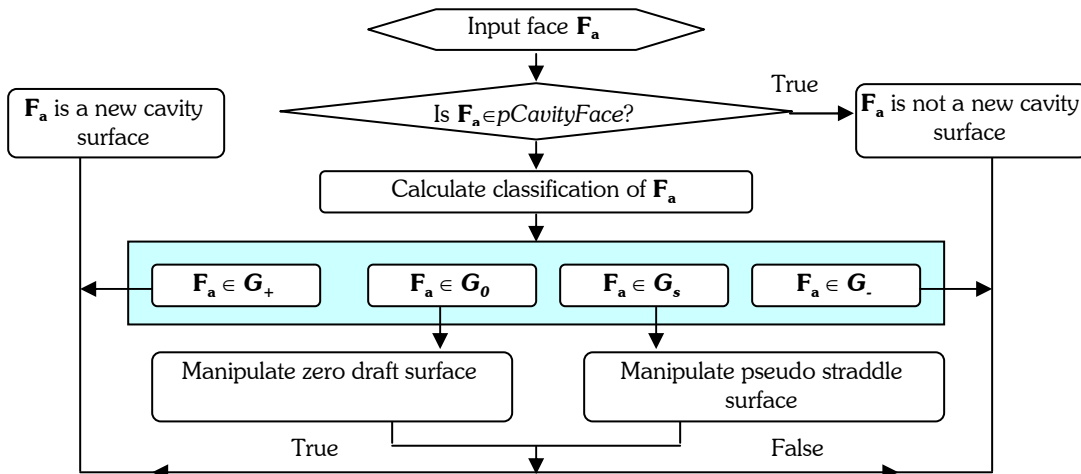
Fig. 4: Algorithm to verify the validity of a new cavity surface.

Using the algorithms described above, a cavity surface group can be identified. By a similar process, a core surface group can also be searched starting from the core seed surface.

3.4.1 Manipulating Pseudo-Straddle Surface

In an ideal geometry model, a G_s straddle surface is always an undercut surface. However, it is not always true in industrial products with complex free-form surfaces or geometrical imperfections. Therefore, a concept of pseudo-straddle surface is introduced so as to improve the parting result for industrial products. Furthermore, a pseudo-straddle surface could be identified as a cavity surface or a core surface by adjusting the given moulding accuracy and geometry tolerance at P_{D+} or P_{D-} respectively.

To define a pseudo-straddle surface, four key parameters are first defined as belows:

<u>Parameter 1</u>: $A_+ = \sum A_i$ for $i=1,2,…k$. Where A_i is the area of ith triangular piece, whose normal vector is N_i and satisfies $N_i \bullet P_{D+} > 0$. Therefore, A_+ is the total area of the surface where its normal vector components are towards P_{D+} and thus can be drawn at P_{D+}.

<u>Parameter 2</u>: $A_- = \sum A_j$ for $j=1,2,…l$. Where A_j is the area of jth triangular piece, whose normal vector is N_j and satisfies $N_j \bullet P_{D-} > 0$. Thus, A_- is total area of the surface where its normal vector components are towards P_{D-} and thus can be drawn at P_{D-}.

<u>Parameter 3</u>: $\alpha_+ = \max\{\alpha_i\}$ for $i=1,2,…k$. Where, $\alpha_i = N_i \bullet P_{D+}$ and satisfies $N_i \bullet P_{D+} > 0$. It is the vector product between P_{D+} and the surface normal vector of the ith triangular piece. Geometrically, α_+ represents the closest surface normal to P_{D+}.

<u>Parameter 4</u>: $\alpha_- = \max\{\alpha_j\}$ for $j=1,2,…l$. Where, $\alpha_j = N_j \bullet P_{D-}$ satisfies $N_j \bullet P_{D-} > 0$. Thus, α_- represents the closest surface normal to P_{D-}.

If a straddle surface satisfies one of the two below conditions expressed by Eqn. (3.3) and Eqn. (3.4), it is then a pseudo-straddle surface. Or else it will be considered as a real undercut surface.

$$A_- < AOA \cap \alpha_- < COS(AOD) \cap F_{\text{int}ersect}(S,R,P_{D+}) \equiv NULL \tag{3.3}$$

$$A_+ < AOA \cap \alpha_+ < COS(AOD) \cap F_{\text{int}ersect}(S,R,P_{D-}) \equiv NULL \tag{3.4}$$

Where, AOA is the area accuracy and AOD the draft angle accuracy given by the moulded product.

If a pseudo-straddle surface satisfies Eqn. (3.3) and is adjacent to any defined cavity surface, it can be identified as a cavity surface. While, if a pseudo-straddle surface satisfies Eqn. (3.4) and is adjacent to any defined core surface, it could be identified as a core surface.

3.4.2 Manipulating Zero Draft Surface

If a undefined zero draft surface **F** can move away from P_{D+} without any obstacle surfaces $F_{intersect}$ as expressed by Eqn. (3.5), it can be set as a new cavity surface during parting process, while it can be set as a new core surface if it can be removed away towards P_{D-} without any obstacle surfaces $F_{intersect}$ expressed by Eqn. (3.6).

$$F \in G_0 \cap F_{\text{int}ersect}(S,R,P_{D+}) \equiv NULL \tag{3.5}$$

$$F \in G_0 \cap F_{\text{int}ersect}(S,R,P_{D-}) \equiv NULL \tag{3.6}$$

The approach to find $F_{intersect}$ is similar as the way described in section 2. The only difference is the way to generate the array of rays R because the projected region R_P of a G_0 surface onto a plane perpendicular to P_D is now a 2D curve rather than a 2D region. In this case, a region R_P is created by offsetting the 2D projected curve of **F** by a length AOL along its normal direction. AOL is a pre-defined length of gap for a moulding. Subsequently, the array of rays R can be generated from this offset region using the same approach as illustrated in section 2.2.

3.5 Identification of Parting Lines

After the cavity and core surface groups have been identified in the previous process, all parting line loops can be extracted accordingly. As shown in Fig. 2, the identification of parting lines includes four steps:

<u>Step 1</u>: Since all the surfaces of the cavity surface group and the core surface group are connected with each other, all boundary loops on cavity side and core side can be easily extracted and are stored into two nominated loop lists, i.e. *plCavityLoop* and *plCoreLoop* respectively.

<u>Step 2:</u> Two potential **OPL** loops are then found from *plCavityLoop* and *plCoreLoop* respectively by comparing the projection area A of each loop onto a plane perpendicular to $\boldsymbol{P_D}$. The loop with the maximum projection area is the preferred **OPL** loop. The equation to compute the projection area A of a loop is expressed as:

$$A = \sum_{k=1}^{n}(x_i y_{i+1} - x_{i+1}y_i) \qquad \text{for } i=0,1,2,\dots m\text{-}1 \qquad (3.7)$$

Where, n represents the number of edges in a loop. (x_i , y_i) is the coordinate of ith point of the kth edge. m is the number of represented points of the kth edge. As for a linear edge, m equals to 2. For other kind of edges, m is determined using the tessellation process on an edge. It is noted that a coordinate transformation from $\boldsymbol{P_D}$ to Z axis must be done to use Eqn. (3.7) if $\boldsymbol{P_D}$ is different from Z axis in the model.

As a result, a cavity **OPL** loop *oplCavityLoop* and a core **OPL** loop *oplCoreLoop* are found. The other parting line loops are therefore known as **IPL** loops.

<u>Step 3:</u> It is known that there is only one **OPL** loop in a moulding. Thus, *oplCavityLoop* and *oplCoreLoop* have to be compared and optimized further to obtain the unique **OPL** loop if they are not same. The preferred **OPL** is determined in terms of the flatness factor. The loop which has the larger flatness factor will be the final **OPL** loop. The flatness factor C_f is expressed in the below equations.

$$C_f = L_{2D} / L_{3D} \qquad (3.8)$$

$$L_{3D} = \sum L_i \qquad \text{for } i=0,1,2\dots nEdge \qquad (3.8\ a)$$

$$L_{2D} = \sum L_i^{2D\_\text{Projection}} \qquad \text{for } i=0,1,2\dots nEdge \qquad (3.8\ b)$$

Where, L_{3D} represents the total length of the parting lines at 3D space, while L_{2D} represents the total length of the parting lines in 2D projection onto the plane perpendicular to $\boldsymbol{P_D}$. L_i is the 3D length of ith edge and $L_i^{2D\_\text{Projection}}$ is 2D projected length. *nEdge* is the total number of edges in the loop.

<u>Step 4:</u> As for the optimization of other **IPL** loops, there are three cases and each case will be processed individually. (1) If a cavity **IPL** loop or a core **IPL** loop is not connected and do not intersect with other core **IPL** loops or cavity **IPL** loops. It is set as a final **IPL** loop. (2) If a cavity **IPL** loop or a core **IPL** loop is exactly same as another core **IPL** loop or cavity **IPL** loop, then the core **IPL** loop will be removed and the cavity **IPL** loop is maintained as the final **IPL** loop. (3) If a cavity **IPL** loop or a core **IPL** loop is intersected with another core **IPL** loop or cavity **IPL** loop, then the flatness factor C_f in Eqn. (3.8) will be used to identify the optimal **IPL** loop.

4. IMPLEMENTATION AND CASE STUDY

The parting methodology introduced in the paper has been implemented based on the SolidWorks platform. All algorithms are developed using Visual C++ as a COM Add-in application. Here, two case studies are given.

Fig. 5(a) shows a plastic moulded part with a few inner parting line loops and an undercut feature. Based on the parting approach, a cavity seed surface and a core seed surface are first identified as shown in Fig. 5(b) and 5(c). Next, the cavity surface group and the core surface group are searched in turn using the iterative surface growth algorithm. The results are shown in Fig. 5(d) and 5(e). In the process of parting lines identification, all tentative parting line loops are first collected from the cavity surface group and the core surface group respectively in Fig. 5(f). However, it was found that there exist two branches in tentative **OPL** loops. Therefore, the optimization is processed based on the flatness criterion. Fig. 5(g) gives the result of the **OPL** and **IPL**. The undercut feature is finally extracted in Fig. 5(h).

Fig. 6(a) gives another moulded product. The part has some zero draft surfaces located at the vertical sides of the slots and a few surfaces with imperfect draft angle as shown in Fig. 6(a) and 6 (b). From the result of draft analysis in Fig. 6(b1), it is found that these surfaces are not perfect $\boldsymbol{G}$ surfaces since the small region Ψ of the surfaces does not

satisfy $N_i \bullet P_{D-} > 0$, but $N_i \bullet P_{D+} > 0$. However, they satisfy the definition of a pseudo-straddle surface proposed in this paper. Based on the proposed approach, a cavity seed face and core seed face are obtained as shown in Fig. 6(c) and (d) respectively. Then, the cavity face group and the core face group are defined using the iterative surface growth algorithm. These zero draft surfaces are identified as cavity surfaces and the highlighted pseudo-straddle surfaces are reasonably identified as core surfaces in terms of the proposed criteria. Fig. 6(e) and 6 (f) shows the result of the cavity surface group and core surface group. Subsequently, the **OPL** loop and **IPL** loops are determined using proposed approach. In this part, the tentative parting line loops extracted from both the cavity side and the core side are the same. The results of **OPL** loop and a few **IPL** loops are highlighted in Fig. 6(g). Finally, all the remaining undefined surfaces are identified as a single undercut feature since they are isolated by two inner parting loops and connected with each other shown in Fig. 6(h). Now, the part has been well split.
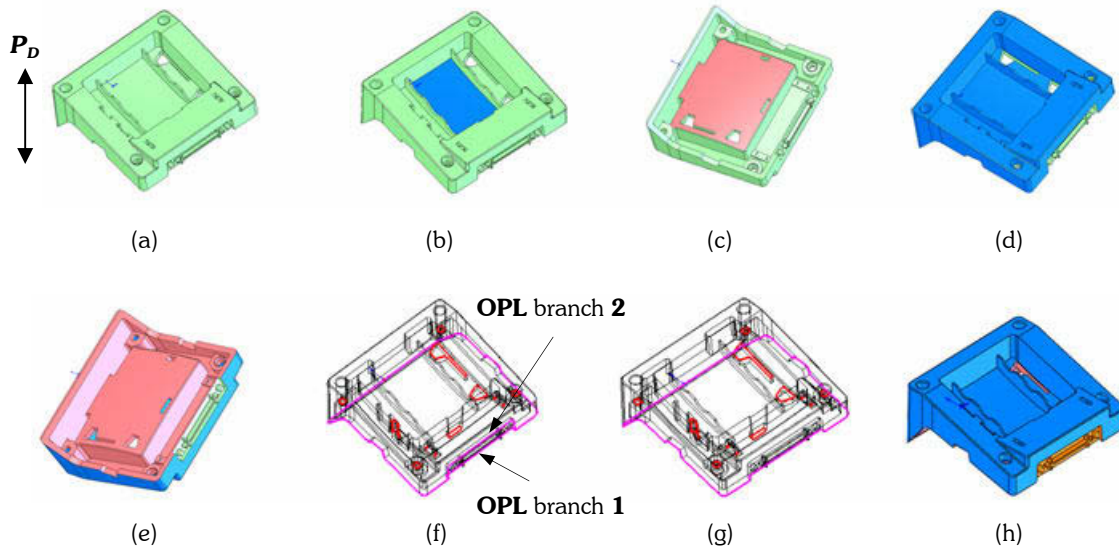
Fig. 5: Case study 1 for proposed parting methodology - (a) product model, (b) cavity seed surface in blue, (c) core seed surface in pink, (d) cavity surface group, (e) core surface group, (f) tentative **OPL**s and **IPL**s, (g) final **OPL** and **IPL**s, (h) undercut feature in orange.

(e)　　　　　　　　(f)　　　　　　　　(g)　　　　　　　　(h)
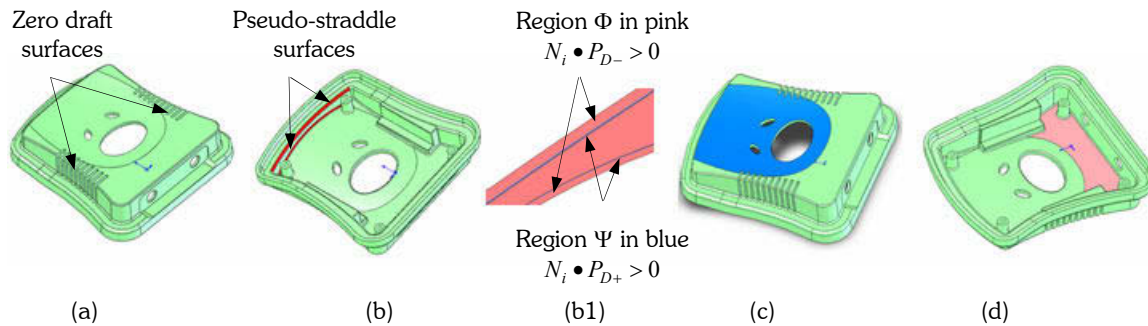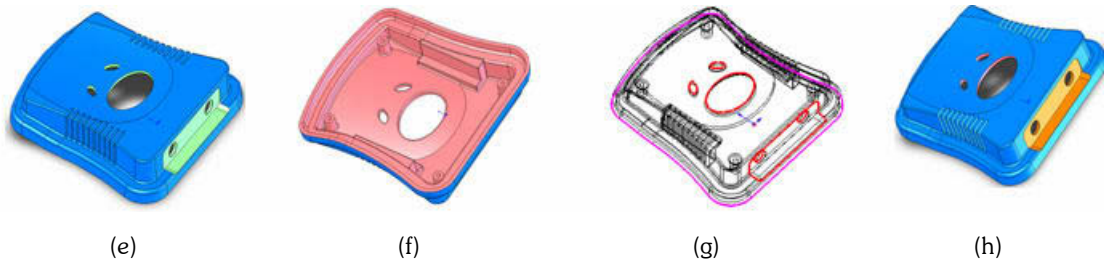
Fig. 6: Case study 2 for proposed parting methodology - (a) product model, (b) pseudo-straddle surfaces, (b1) draft analysis result of pseudo-straddle surfaces (c) cavity seed surface in blue, (d) core seed surface in pink, (e) cavity surface group, (f) core surface group, (g) final **OPL** and **IPL**s, (h) undercut feature in orange.

5. SUMMARY AND CONCLUSION

The case studies show that the parting methodology presented in the paper is robust and effective for automatically identifying outer parting loop, inner parting line loops, cavity/core surfaces and undercut features for complex moulded products in an mould design system. Compared to other parting methodologies, the proposed approach is robust for free-form surfaces and complex geometry structures since the approach is fully dependent on the geometry visibility and mouldability and thus independent of the complexity of feature structure. The concept of pseudo-straddle surface is introduced to manipulate geometry and draft angle imperfections commonly resulting from data transferred among different CAD applications so that the approach can give satisfactory results for various industrial products.

The limitation of the proposed methodology is found in a case due to the presence of a special convex undercut feature as illustrated in Fig. 7 (a). Based on the proposed parting approach, the surface $\mathbf{F}1$ and $\mathbf{F}2$ will be assigned as undercut surfaces since they are not able to be drawn away from both $\boldsymbol{P_{D+}}$ and $\boldsymbol{P_{D-}}$ in Fig. 7 (a1). However, the surface $\mathbf{F}3$ and $\mathbf{F}4$ are assigned as a cavity surface and a core surface respectively. In other words, the entire undercut feature cannot be detected successfully. There are two ways to resolve the problem, i.e. (i) further recognition of the entire convex undercut feature using graph-based methods [1], [3], [7], [8] and [11], and (ii) revision of the design by splitting associated surfaces as indicated in Fig. 7(a2).

(a)　　　　　　　　　　　(a1)　　　　　　　　　　(a2)
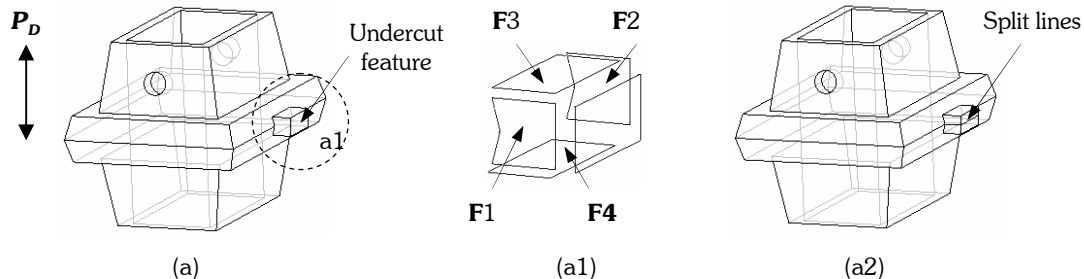
Fig. 7: The limitations of the parting methodology due to the presence of convex undercut features.

6. REFERENCES

[1]	Emad, S. Abouel Nasr; Kamrani, Ali K.: A new methodology for extracting manufacturing features from CAD system, Computers & Industrial Engineering, 51(3), 2006, 389-415.

[2]	Fu, M. W.; Nee, A. Y. C.; Fuh, J. Y. H.: The application of surface visibility and mouldability to parting line generation, Computer-Aided Design, 34(6), 2002, 469-480.

[3]	Fu, M. W.; Fuh, J. Y. H.; Nee, A. Y. C: Undercut feature recognition in an injection mould design system, Computer-Aided Design, 31(12), 1999, 777-790.

[4]	Gan, J. G.; Woo, T. C.; Tang, K.: Spherical Maps: their construction, properties, and approximation, ASME Journal of Mechanical Design, 116, 1994, 3573.

[5] Paramio, M. A. R.; Garcia, J. M. P.; Chueco, J. R.; Idoipe, A. V.; Sevillano, J.J.M.: A procedure for plastic parts demoldability analysis, Robotics and Computer-Integrated Manufacturing, 22(1), 2006, 81-92.

[6] Nee, A. Y. C.; Fu, M. W.; Fuh, J. Y. H.; Lee, K. S.; Zhang, Y. F.: Automatic determination of 3-D parting lines and surfaces in plastic injection mould, Annals of CIRP, 47 (1), 1998, 95-98.

[7] Gavankar, P.; Henderson, M. R.: Graph-based extraction of protrusions and depressions from boundary representations, Computer-Aided Design, 22(7), 1990, 442-450.

[8] Pal. P.; Tigga, A. M.; Kumar, A: Feature extraction from large CAD databases using genetic algorithm, Computer-Aided Design, 37(5), 2005, 545-558.

[9] Tan, S. T.; Yuen, M. F.; Sze, W. S.; Kwong, W. K.: Parting lines and parting surfaces of injection moulded parts, Proc. Instn Mech. Engrs, 204, 1990, 201-219.

[10] Weinstein; Manoochehri, S.: Optimum parting line design of moulded and cast parts for manufacturability, Journal of Manufacturing Systems, 16, 1997, 1-12.

[11] Ye, X. G.; Fuh, J. Y. H.; Lee, K. S: A hybrid method for recognition of undercut features from moulded parts, Computer-Aided Design, 33(14), 2001, 1023-1034.